

Article

High-Pressure and High-Temperature Phase Transitions in Fe_2TiO_4 and Mg_2TiO_4 with Implications for Titanomagnetite Inclusions in Superdeep Diamonds

Masaki Akaogi *, Taisuke Tajima, Masaki Okano and Hiroshi Kojitani

Department of Chemistry, Gakushuin University, Mejiro, Toshima-ku, Tokyo 171-8588, Japan

* Correspondence: masaki.akaogi@gakushuin.ac.jp; Tel.: +81-3-5904-9377; Fax: +81-3-5992-1029

Received: 8 September 2019; Accepted: 3 October 2019; Published: 6 October 2019



Abstract: Phase transitions of Mg_2TiO_4 and Fe_2TiO_4 were examined up to 28 GPa and 1600 °C using a multianvil apparatus. The quenched samples were examined by powder X-ray diffraction. With increasing pressure at high temperature, spinel-type Mg_2TiO_4 decomposes into MgO and ilmenite-type MgTiO_3 which further transforms to perovskite-type MgTiO_3 . At ~21 GPa, the assemblage of MgTiO_3 perovskite + MgO changes to $2\text{MgO} + \text{TiO}_2$ with baddeleyite (or orthorhombic I)-type structure. Fe_2TiO_4 undergoes transitions similar to Mg_2TiO_4 with pressure: spinel-type Fe_2TiO_4 dissociates into FeO and ilmenite-type FeTiO_3 which transforms to perovskite-type FeTiO_3 . Both of MgTiO_3 and FeTiO_3 perovskites change to LiNbO_3 -type phases on release of pressure. In Fe_2TiO_4 , however, perovskite-type FeTiO_3 and FeO combine into calcium titanate-type Fe_2TiO_4 at ~15 GPa. The formation of calcium titanate-type Fe_2TiO_4 at high pressure may be explained by effects of crystal field stabilization and high spin–low spin transition in Fe^{2+} in the octahedral sites of calcium titanate-type Fe_2TiO_4 . It is inferred from the determined phase relations that some of Fe_2TiO_4 -rich titanomagnetite inclusions in diamonds recently found in São Luiz, Juina, Brazil, may be originally calcium titanate-type Fe_2TiO_4 at pressure above ~15 GPa in the transition zone or lower mantle and transformed to spinel-type in the upper mantle conditions.

Keywords: phase transition; high pressure; Mg_2TiO_4 ; Fe_2TiO_4 ; spinel; ilmenite; perovskite; lithium niobate; calcium titanate; diamond inclusion

1. Introduction

Titanomagnetite ($\text{Fe}_{3-x}\text{Ti}_x\text{O}_4$), one of the important magnetic minerals in igneous and metamorphic rocks, is a solid solution between Fe_3O_4 magnetite ($x = 0$) and Fe_2TiO_4 ulvöspinel ($x = 1$), formed by replacement of Fe^{3+} by Ti^{4+} . Fe_2TiO_4 ulvöspinel has an inverse spinel structure where tetrahedral sites are occupied by Fe^{2+} and octahedral sites are occupied randomly by Fe^{2+} and Ti^{4+} [1,2]. Mg_2TiO_4 qandilite is one of endmembers of spinel solid solution in the system Fe_2TiO_4 – Mg_2TiO_4 – Fe_3O_4 – MgFe_2O_4 , and is important in industrial ceramics. Mg_2TiO_4 qandilite also has the inverse spinel structure [3]. High-pressure phase transitions of $A_2\text{BO}_4$ and $AB_2\text{O}_4$ spinels have received much attention in geophysics and mineral physics, because they provide valuable information on post-spinel transitions of spinel-structured Mg_2SiO_4 ringwoodite which occurs at 660 km depth in the mantle and on stability of aluminous phases with the $AB_2\text{O}_4$ stoichiometry in the deep mantle.

Phase transitions of Fe_2TiO_4 spinel at room temperature and high pressure have been studied in detail [2,4–6]. The studies indicated that at room temperature Fe_2TiO_4 cubic spinel (space group $Fd\bar{3}m$) first changes into tetragonal spinel ($I4_1/adm$) at 9 GPa due to a Jahn-Teller effect of Fe^{2+} in the tetragonal site. At 12 GPa, the tetragonal spinel transforms to CaTi_2O_4 -type structure ($Cmcm$), in which octahedral

sites are occupied by disordered Fe^{2+} and Ti^{4+} and eight-fold sites by Fe^{2+} . The CaTi_2O_4 -type Fe_2TiO_4 further transforms at 53 GPa to another high-pressure polymorph (*Pmma*) with ordered Fe^{2+} and Ti^{4+} in the octahedral sites. Yamanaka et al. [4] reported that the high spin-low spin transition in Fe^{2+} in the octahedral sites of the CaTi_2O_4 -type Fe_2TiO_4 started to occur above about 15 GPa at room temperature and that all of Fe^{2+} in the octahedral sites were in the low spin state in the *Pmma* phase, while Wu et al. [6] reported that the spin transition in Fe^{2+} initiated at around 40 GPa.

In contrast, studies on high-pressure and high-temperature transitions of Fe_2TiO_4 and Mg_2TiO_4 spinels have been limited. Phase transitions of the spinels were examined only up to 5 GPa at 800–1600 °C by Akimoto and Syono [7]. They reported that both Fe_2TiO_4 and Mg_2TiO_4 spinels decompose into $A\text{TiO}_3$ ilmenite and AO with rock-salt structure ($A = \text{Mg}, \text{Fe}$). The phase transitions at high temperature and high pressure above ~5 GPa, however, have not been well examined so far. Changes in elastic properties associated with the phase transitions in Fe_2TiO_4 and Mg_2TiO_4 shown above were investigated by Liebermann et al. [8]. The physical basis of elastic properties at high pressure and high temperature is described in detail by Anderson [9].

In this study, we have investigated phase transitions in Fe_2TiO_4 and Mg_2TiO_4 up to 28 GPa and 1600 °C, using a Kawai-type multianvil apparatus. We have found that the transition sequences in Fe_2TiO_4 at high pressure and high temperature are substantially different from those at high pressure and room temperature. Based on the results on Fe_2TiO_4 and Mg_2TiO_4 , we discuss the difference in the transition behaviors between Fe_2TiO_4 and Mg_2TiO_4 from a crystal–chemical point of view. In addition, we discuss stability and possible origin of Fe_2TiO_4 -rich titanomagnetites which were found as inclusions in superdeep diamonds from Juina area, Brazil [10,11].

2. Experimental Methods

Starting materials for high-pressure and high-temperature experiments of Mg_2TiO_4 and Fe_2TiO_4 were synthesized as follows. Spinel(Sp)-type Mg_2TiO_4 (qandilite) was synthesized from a 2:1 mixture (molar ratio) of MgO (>99.9% purity, Wako Co., Osaka, Japan) and TiO_2 (>99.9%, Wako Co.) by heating at 1300 °C for 20 h. Sp-structured Fe_2TiO_4 (ulvöspinel) was synthesized from a 1:1 mixture of Fe_2O_3 (>99.9%, Wako Co.) and TiO_2 by heating at 1270 °C for 27 h in controlled oxygen fugacity with mixed gasses of CO_2 , H_2 and Ar (3:2:5 volume ratios). Powder X-ray diffraction measurements and composition analyses using a scanning electron microscope (SEM) with an energy-dispersive X-ray spectrometer (EDS) indicated that the synthesized samples were single-phase Sp-type Mg_2TiO_4 and Fe_2TiO_4 with the stoichiometric compositions. The lattice parameters determined by powder X-ray diffraction were $a = 8.4398(1)$ Å for Mg_2TiO_4 Sp and $a = 8.5375(3)$ Å for Fe_2TiO_4 Sp, which were in good agreement with those by Wechsler et al. [3] and Wechsler et al. [1], respectively. For high-pressure and high-temperature experiments of Fe_2TiO_4 , 5 wt % metallic iron (>99.9 %, Johnson Matthey Co., London, UK) was added to the above synthesized Fe_2TiO_4 Sp to keep iron in the Fe_2TiO_4 samples in ferrous state.

High-pressure and high-temperature experiments were performed with the quench method using a Kawai-type 6-8 multianvil apparatus [12] at Gakushuin University. Tungsten carbide anvils with 2.5 mm truncated edge-length were used as the second-stage anvils. A 5 wt % Cr_2O_3 -doped MgO octahedron of 7 mm edge length was used as the pressure medium. A cylindrical Re heater was placed in the central part of the octahedron. For the experiments of Mg_2TiO_4 , the powdered starting material was directly put into the Re heater. For thermal insulation, a LaCrO_3 sleeve was placed between the heater and the MgO octahedron along with two LaCrO_3 plugs in both ends of the furnace. Two Pt discs were placed between the sample and the plugs to avoid any reaction between them. For the experiments of Fe_2TiO_4 , the mixture of 95 wt % Fe_2TiO_4 and 5 wt % Fe was put into an Fe capsule which was placed in the central part of the Re heater. A BN sleeve was inserted between the Fe capsule and Re heater for electrical insulation. Temperature was measured at the central part of the outer surface of the furnace with a Pt/Pt-13%Rh thermocouple. Effect of pressure on emf of the thermocouple was ignored.

Pressure was calibrated at room temperature using pressure-fixed points: Bi I-II (2.55 GPa), Bi III-V (7.7 GPa), ZnS (15.6 GPa), and GaAs (18.3 GPa) in Ito [12] and GaP (23 GPa) by Dunn and Bundy [13]. The pressure was further corrected at 1200 and 1600 °C, using transition pressures of Mg₂SiO₄ olivine–wadsleyite–ringwoodite [14,15] and MgSiO₃ akimotoite–bridgmanite [16] and decomposition pressure of Mg₃Al₂Si₃O₁₂ pyrope to MgSiO₃-rich bridgmanite + Al₂O₃-rich corundum [16]. Uncertainties of pressure and temperature were estimated to be ±0.3 GPa and ±20 °C, respectively. In each run, pressure was raised to a targeted pressure of 11–28 GPa at a constant rate during about 2–4 h, and then temperature was raised to a targeted temperature of 1000–1600 °C at a rate of about 100 °C/min. The samples were kept for 60–120 min at the pressure-temperature conditions, and then quenched under pressure, slowly decompressed, and recovered to ambient conditions.

The recovered samples were pulverized and examined by a powder X-ray diffractometer (Rigaku, RINT2500, Tokyo, Japan) operated at 45 kV and 250 mA with a rotating Cr anode. Monochromatized CrK α radiation was used for identification of phases in the run products and determination of lattice parameters. High-purity Si powder was used to calibrate 2 θ angle of the powder X-ray diffractometer. The lattice parameters were refined by the least squares method. By using some parts of run products which were mounted on slide-glass plates with epoxy resin and polished flat, phase identification and chemical analysis were made using a SEM (JEOL, JMS-6360, Tokyo, Japan) in combination with an EDS (SGX Sortech Sirius SD-10133, High Wycombe, UK). The SEM was operated with acceleration voltage of 15 kV and probe current of 0.55 nA. Natural forsterite and synthetic fayalite and MnTiO₃ provided by JEOL were used as standard materials for Mg, Fe and Ti, respectively.

3. Results

3.1. Phase Transitions in Mg₂TiO₄

Table 1 summarizes results of phase transition experiments in Mg₂TiO₄ at 21–28 GPa and 1000–1600 °C. The previous study showed that at pressure below 1–2 GPa spinel (Sp)-type Mg₂TiO₄ first dissociates into ilmenite (Ilm)-type MgTiO₃ + MgO periclase (Pc) [7]. Figure 1a shows a powder X-ray diffraction pattern of the run product (No. O161021) quenched from 21 GPa and 1600 °C. The diffraction pattern exhibits MgO Pe and a phase with very similar diffraction peaks to MgTiO₃ Ilm (space group *R*-3). However, some diffraction peaks such as 003 and 101 of MgTiO₃ Ilm in 2 θ range of 20–30° are absent. Almost all the peaks were indexed with hexagonal symmetry, and refined cell parameters were $a = 5.0774(5)$ Å, $c = 13.716(2)$ Å, giving $c/a = 2.701$. This c/a value is considerably smaller than 2.750 of MgTiO₃ Ilm [3]. The diffraction data in Figure 1a and the lattice parameters are consistent with those of LiNbO₃ (Ln)-type MgTiO₃ (*R3c*) [17]. Linton et al. [17] reported that Ilm-type MgTiO₃ transforms at about 15–20 GPa to the perovskite (Pv) phase, which is converted to the Ln-type phase on decompression. Therefore, our results in Table 1 and Figure 1a reveal that MgTiO₃ Pv + MgO Pe are stable at 21 GPa and 1600 °C and that MgTiO₃ Pv transforms to the Ln-type on release of pressure.

Table 1. Results of high-pressure and high-temperature experiments in Mg₂TiO₄.

Run No.	Pressure (GPa)	Temperature (°C)	(min)	Run Product
O160915	21	1000	120	Pe, Ln
O161025	23	1000	90	Pe, α
O161017	21	1300	90	Pe, Ln
O170116	22.5	1300	50	Ln, Pe, α
O161128	23.5	1300	60	Pe, α , Ln(tr)
O160909	24.5	1300	60	Pe, α

Table 1. Cont.

Run No.	Pressure (GPa)	Temperature (°C)	(min)	Run Product
O160924	28	1300	90	Pe, α
O161106	28	1400	90	Pe, α , Ln(tr)
O170219	22	1500	90	Ln, Pe, α
O170202	25	1500	60	Pe, α
O170126	28	1500	60	Pe, α
O161021	21	1600	90	Pe, Ln
O161124	22	1600	60	Pe, Ln
O161209	23.5	1600	60	Ln, Pe, α
O160903	24.5	1600	60	Pe, α , Ln(tr)

Abbreviations are as follows: Ln, LiNbO₃-type MgTiO₃; Pe, MgO periclase; α , α PbO₂ type TiO₂; tr, trace.

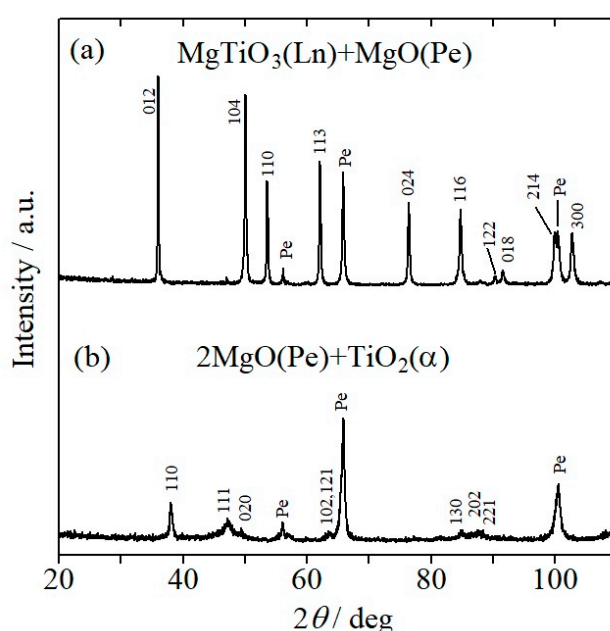


Figure 1. Powder X-ray diffraction patterns (Cr K α) of run products of Mg₂TiO₄, (a) No. O161021 (21 GPa, 1600 °C) and (b) No. O160924 (28 GPa, 1300 °C). Miller indices in (a) are for Ln-type MgTiO₃, and those in (b) are for α PbO₂-type TiO₂. Ln: LiNbO₃-type, Pe: periclase, α : α PbO₂-type.

Figure 1b shows a powder X-ray diffraction pattern of the run product (No. O160924) quenched from 28 GPa and 1300 °C, in which diffraction peaks of MgO Pe and α PbO₂ type TiO₂ are observed. Broad diffraction peaks of α PbO₂ type TiO₂ in Figure 1b suggest that the phase was a retrograde transformation product from a high-pressure phase. Previous studies on TiO₂ indicated that at about 800–1000 °C TiO₂ rutile transforms to α PbO₂ type at about 6–8 GPa, which further transforms to baddeleyite (Bd)-type TiO₂ (akaogiite) [18,19] at about 15–20 GPa [20–22]. The Bd-type TiO₂ transforms to orthorhombic-I (OI) type TiO₂ at about 25–30 GPa at 1200–1500 °C [23,24]. These studies also showed that both of Bd- and OI-type TiO₂ phases back-transform to α PbO₂ type TiO₂ on release of pressure. Therefore, based on the experimental pressure range and the broad X-ray diffraction peaks, we conclude that the α PbO₂ type TiO₂ found in the run products of 28 GPa and 1300 °C was the retrograde transition product from Bd- or OI-type TiO₂ synthesized at the P, T conditions. This leads to the conclusion that MgTiO₃ Pv stable at 21 GPa decomposes to the constituent oxides at higher pressure.

Figure 2 shows the phase diagram of Mg₂TiO₄. Our experimental results at 21–28 GPa and 1000–1600 °C indicate that the transition boundary of MgTiO₃ Pv + MgO Pe to 2MgO Pe + Bd-type TiO₂ which is the decomposition boundary of MgTiO₃ Pv is located at 21–23 GPa and 1000–1600 °C with a small positive dP/dT slope. Figure 2 also includes the dissociation boundary of Mg₂TiO₄ Sp

to MgTiO_3 Ilm + MgO Pe below $\sim 1\text{--}2$ GPa [7], as well as the Ilm-Pv transition boundary of MgTiO_3 at $\sim 15\text{--}20$ GPa [25]. The assemblage of MgO and TiO_2 is stable to at least 35 GPa at 1400°C in our preliminary study on phase transitions in MgTiO_3 [25].

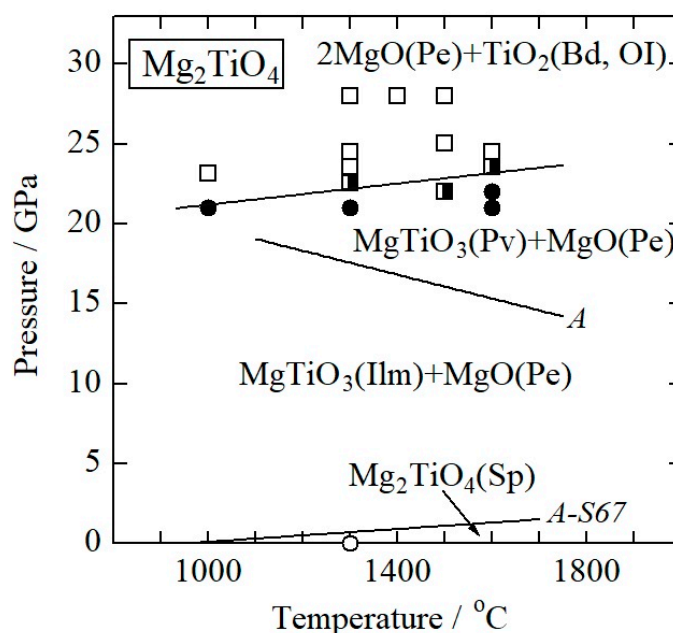
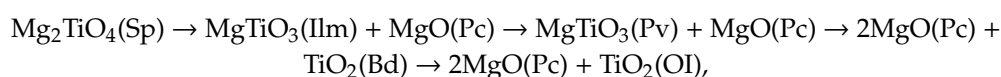


Figure 2. Phase diagram of Mg_2TiO_4 . An open circle: $\text{Mg}_2\text{TiO}_4(\text{Sp})$, solid circles: $\text{MgTiO}_3(\text{Pv}) + \text{MgO}(\text{Pe})$, open squares: $2\text{MgO}(\text{Pe}) + \text{TiO}_2(\text{Bd, OI})$. A thick solid line: this study, a thin line with A-S67: Sp dissociation boundary to Ilm + Pe [7], a thin line with A: Ilm-Pv boundary [25]. Sp: spinel-type, Ilm: ilmenite-type, Pe: periclase, Pv: perovskite-type, Bd: baddeleyite-type, OI: orthorhombic I-type.

Molar volumes of high-pressure phases in the systems MgO-TiO_2 and FeO-TiO_2 are listed in Table 2. Using the data in Table 2, for the following transitions in Mg_2TiO_4 :



we obtain molar volume changes at ambient conditions of -3.15 , -1.55 , -1.17 and -0.07 cm^3/mol , respectively, which are -7.0 , -3.7 , -2.9 and -0.2% , respectively.

3.2. Phase Transitions in Fe_2TiO_4

Results of high-pressure transition experiments in Fe_2TiO_4 are summarized in Table 3. Phase identification was made mostly by powder X-ray diffraction method. Metallic iron in the samples was identified by the SEM-EDS analysis and/or powder X-ray diffraction. Fe_2TiO_4 ulvöspinel first dissociates into Ilm-type FeTiO_3 and FeO wustite (Wu) at $4\text{--}5$ GPa and $1000\text{--}1300^\circ\text{C}$ [7]. Figure 3a shows a powder X-ray diffraction pattern of the run product (No. M150115) synthesized at 14 GPa and 1100°C . The diffraction pattern of Figure 3a is composed of FeO Wu, metallic iron, and the other phase whose diffraction peaks agree with those of Ln-type FeTiO_3 by Akaogi et al. [26]. The Ln-type FeTiO_3 phase is interpreted to be the retrograde transition product from Pv-type FeTiO_3 [27]. Natural occurrences of Ln-type FeTiO_3 were reported in shocked meteorites, and the new mineral was recently named wangdaodeite [28,29].

Figure 3b shows a powder X-ray diffraction pattern of the run product (No. M140710) synthesized at 18 GPa and 1300°C . The diffraction pattern is similar to calcium titanate (CaTi_2O_4), and the peaks were indexed with orthorhombic symmetry (Figure 3b). The Miller indices were consistent with extinction rules of $\text{CaTi}_2\text{O}_4(\text{CT})$ -structured phase ($Cmcm$). The lattice parameters refined using twenty

nine diffraction peaks of the Fe_2TiO_4 phase were $a = 2.9473(5) \text{ \AA}$, $b = 9.6448(2) \text{ \AA}$, $c = 9.9085(2) \text{ \AA}$, $V = 281.663(7) \text{ \AA}^3$. The cell parameters agree well with those extrapolated to ambient pressure of CT-type Fe_2TiO_4 at 38–50 GPa and room temperature by Yamanaka et al. [4]. These results indicate that the Fe_2TiO_4 phase in the run product synthesized at 18 GPa and 1300 °C is the CT-type phase. This is consistent with the results in the previous studies that Fe_2TiO_4 CT is quenchable at ambient conditions [5,30]. Compositions of coexisting Fe_2TiO_4 CT and FeTiO_3 Ln with very small grains of FeO Wu in the run product (No. M140626) at 15 GPa and 1300 °C were analyzed using the SEM-EDS: $\text{Fe}_{1.97(1)}\text{Ti}_{1.01(1)}\text{O}_4$ for CT-type phase and $\text{Fe}_{0.95(2)}\text{Ti}_{1.02(1)}\text{O}_3$ for Ln-type phase, indicating almost stoichiometric compositions within the analytical errors.

Table 2. Molar volumes of phases in the systems MgO-TiO₂ and FeO-TiO₂.

Comp.	Structure	V ₀ (cm ³ /mol)	Ref.	Comp.	Structure	V ₀ (cm ³ /mol)	Ref.
MgO	rock-salt	11.24	a	FeO	rock-salt	12.17	i
MgTiO ₃	ilmenite	30.86	b	FeTiO ₃	ilmenite	31.72	j
MgTiO ₃	perovskite	29.31	c	FeTiO ₃	perovskite	30.34	k
MgTiO ₃	LiNbO ₃	30.71	d	FeTiO ₃	LiNbO ₃	31.34	j
Mg ₂ TiO ₄	spinel	45.25	e	Fe ₂ TiO ₄	spinel	46.84	e
TiO ₂	αPbO ₂	18.41	f	Fe ₂ TiO ₄	CaTi ₂ O ₄	42.41	e
TiO ₂	baddeleyite	16.90	g				
TiO ₂	OI	16.83	h				

V₀: molar volume at ambient conditions. Ref. a: Hazen [31], b: Wechsler and Von Dreele [3], c: Linton et al. [17], d: Linton et al. [32], e: This study, f: Kojitani et al. [22], g: Al-Khatatbeh et al. [24], h: Nishio-Hamane et al. [33], i: McCammon [34], j: Akaogi et al. [26], k: Leinenweber et al. [27].

Table 3. Results of high-pressure and high-temperature experiments in Fe_2TiO_4 .

Run no.	Pressure (GPa)	Temperature (°C)	Time (min)	Run Product *
M150109	12.5	1000	60	Ilm, Wu
M150107	12.5	1100	60	Ilm, Wu
M140806	13	1100	60	Ilm, Ln, Wu
M150115	14	1100	60	Ln, Wu
M141128	15.5	1100	60	Ln, Wu
M140707	16	1100	60	CT
M150218	17	1100	60	CT
M150603	20	1100	60	CT
M150226	23	1100	60	CT
M150516	24	1100	60	CT
M150127	12.5	1200	60	Ilm, Ln, Wu
M150416	18	1200	60	CT
M150707	11	1300	60	Ilm, Wu
M150725	12	1300	60	Ilm, Wu
M140728	13	1300	60	Ln, Wu
M150625	14	1300	60	Ln, Wu
M150202	15	1300	60	CT
M140626	15	1300	60	CT, Ln, Wu
M140701	18	1300	60	CT
M140710	18	1300	60	CT
M150227	20	1300	60	CT
M150606	22	1300	60	CT

* Metallic iron coexisted in the run products. Ilm: ilmenite-type FeTiO_3 , Wu: FeO wustite, Ln: LiNbO₃-type FeTiO_3 , CT: CT-type Fe_2TiO_4 .

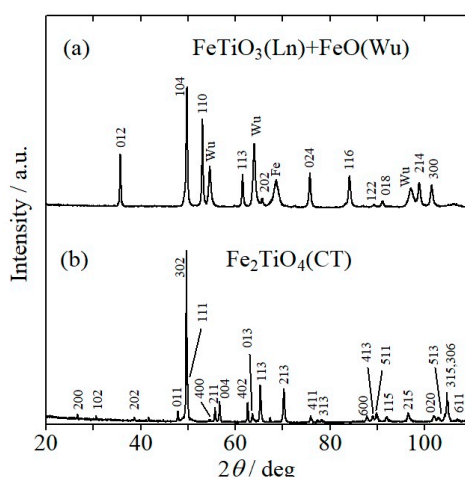


Figure 3. Powder X-ray diffraction patterns (Cr $K\alpha$) of run products of Fe_2TiO_4 , (a) No. M150115 (14 GPa, 1100 °C) and (b) No. M140710 (18 GPa, 1300 °C). Miller indices in (a) are for Ln-type $FeTiO_3$, and those in (b) are for CT-type Fe_2TiO_4 . Ln: $LiNbO_3$ -type, Wu: wustite, Fe: metallic iron, CT: calcium titanate-type.

Figure 4 shows the phase diagram of Fe_2TiO_4 . Our experimental results indicate that at 1000–1300 °C the assemblage of FeO Wu + $FeTiO_3$ Ln which was Pv at high P, T was observed in the run products synthesized at 12.5–15.5 GPa, while FeO Wu + $FeTiO_3$ Ilm was observed at 11–12.5 GPa. The Ilm-Pv transition boundary has a small negative slope. The Ilm-Pv transition pressure in this study is generally consistent with that obtained by extrapolation of the boundary determined at 500–900 °C by Ming et al. [35]. We found that the assemblage of $FeTiO_3$ Ln (Pv at high P, T) and FeO Wu changes to Fe_2TiO_4 CT in the run products at 15–16 GPa at 1100–1300 °C with a small negative slope boundary. Therefore, the stability field of $FeTiO_3$ Pv and FeO Wu is limited in a narrow pressure interval of about 2 GPa. This study indicates that Fe_2TiO_4 CT is stable up to at least 22–24 GPa at 1100–1300 °C. In our previous study in $FeTiO_3$ composition, we found that Fe_2TiO_4 CT coexists with OI-type TiO_2 up to about 33 GPa, above which it decomposes into FeO Wu + TiO_2 OI [26]. Therefore, the upper stability pressure of Fe_2TiO_4 CT is about 33 GPa.

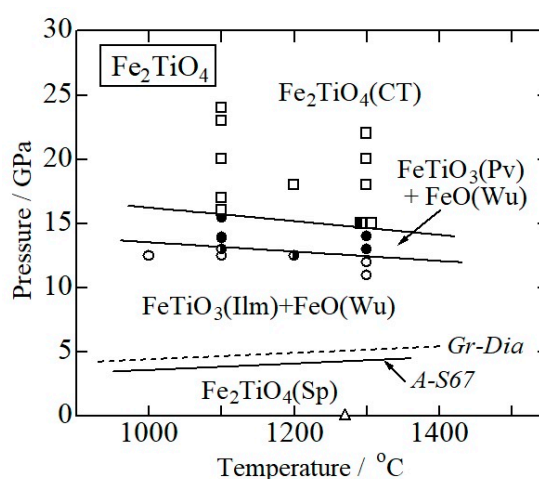
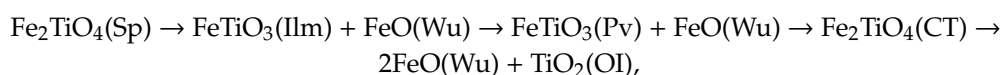


Figure 4. Phase diagram of Fe_2TiO_4 . An open triangle: Fe_2TiO_4 (Sp), open circles: $FeTiO_3$ (Ilm) + FeO(Wu), solid circles: $FeTiO_3$ (Pv) + FeO(Wu), open squares: Fe_2TiO_4 (CT). Thick solid lines: this study, a thin line with A-S67: Sp dissociation boundary to Ilm + Wu [7], a thin dashed line with Gr-Dia: the graphite–diamond boundary [36]. Sp: spinel-type, Ilm: ilmenite-type, Wu: wustite, Pv: perovskite-type, CT: calcium titanate-type.

The results in Figure 4 combined with those by Akaogi et al. [26] indicate that the following transitions occur in Fe₂TiO₄ with increasing pressure:



where molar volume changes at ambient conditions are -2.95 , -1.38 , -0.10 and -1.24 cm³/mol, which are -6.3% , -3.1% , -0.2% and -2.9% , respectively, using the data in Table 2.

4. Discussion

Our results indicate that Fe₂TiO₄ Sp undergoes phase transitions to FeTiO₃ Ilm + FeO Wu and subsequently to FeTiO₃ Pv + FeO Wu at high pressure and high temperature (Figure 4). The decomposition of Fe₂TiO₄ Sp to FeTiO₃ Ilm + FeO Wu is consistent with the result by Akimoto and Syono [7]. However, at room temperature and high pressure, the transition behavior is different: Fe₂TiO₄ cubic Sp is distorted to tetragonal Sp at ~ 9 GPa due to the Jahn-Teller effect of Fe²⁺ at the tetrahedral site [2]. The difference may arise from kinetic hindrance to decomposition into FeTiO₃ Ilm + FeO Wu at room temperature. In the experiments at room temperature and high pressure, tetragonal Sp transforms to Fe₂TiO₄ CT at ~ 15 GPa [4,6]. The pressure is generally consistent with transition pressure to Fe₂TiO₄ CT at room temperature extrapolated from the results at 1000–1300 °C, considering the uncertainty of the boundary slope (Figure 4).

Here, we compare the transitions in Mg₂TiO₄ and Fe₂TiO₄. As shown in Figures 2 and 4, both of Sp-type Mg₂TiO₄ and Fe₂TiO₄ dissociate into ATiO₃ Ilm and AO ($A = \text{Mg, Fe}$) at pressures below ~ 5 GPa, and both of the ATiO₃ Ilm transform to ATiO₃ Pv at ~ 13 – 15 GPa. At higher pressure, however, the transition behaviors are different between Mg₂TiO₄ and Fe₂TiO₄. In Mg₂TiO₄, the assemblage of MgTiO₃ Pv + MgO Pe changes into 2MgO Pe + TiO₂ Bd due to decomposition of MgTiO₃ Pv. However, in Fe₂TiO₄ the assemblage of FeTiO₃ Pv + FeO Wu changes at ~ 15 GPa to CT-type Fe₂TiO₄ which is stable up to ~ 33 GPa.

Figure 5 illustrates the CT-type structure (*Cmcm*). The structure consists of double chains of edge-sharing octahedra running parallel to the a-axis, and tunnel spaces are formed by four corner-sharing double chains [37,38]. In the structure of CT-type Fe₂TiO₄, Fe²⁺ and Ti⁴⁺ are randomly distributed in the octahedral sites and only Fe²⁺ in the eight-fold sites in the tunnel spaces. Compared with Mg₂TiO₄, crystal-field effect of Fe²⁺ in the octahedral sites may stabilize the CT-type phase of Fe₂TiO₄ composition. Using effective ionic radii by Shannon [39], the difference of ionic radii between Fe²⁺ (0.78 Å in high-spin state) and Ti⁴⁺ (0.605 Å) in octahedral site is larger than that between Mg²⁺ (0.72 Å) and Ti⁴⁺. However, the ionic radius of Fe²⁺ in low-spin state in the octahedral site is 0.61 Å, which is much closer to that of Ti⁴⁺ compared with Mg²⁺. When we adopt that the high-spin to low-spin transition of Fe²⁺ in the octahedral site of Fe₂TiO₄ CT starts to occur at pressure of ~ 15 – 20 GPa at room temperature and proportion of low-spin Fe²⁺ increases with pressure [4], it is suggested that the very similar ionic radii of low-spin Fe²⁺ and Ti⁴⁺ is more favorable for the CT-type structure. Although the high-spin state and low-spin state would be mixed at high temperature such as 1000–1300 °C [40], it is likely that both of the crystal-field effect and the high-spin to low-spin transition of Fe²⁺ may facilitate the stability of Fe₂TiO₄ CT above ~ 15 GPa.

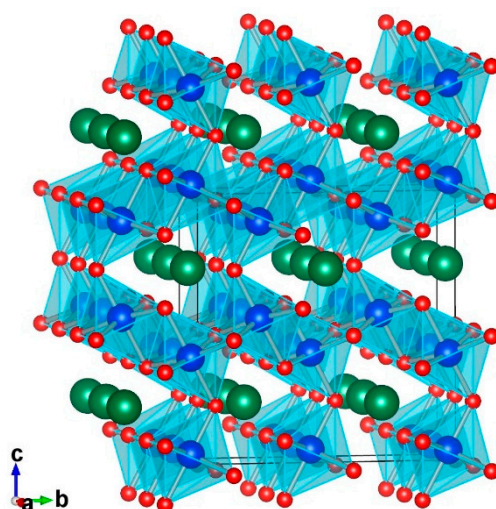


Figure 5. Crystal structure of CaTi_2O_4 -type AB_2O_4 . Small red spheres, middle blue ones and large green ones express oxygen, B and A cations, respectively. The structure was drawn by VESTA [41].

Sp-type titanomagnetites were found as inclusions in diamonds from some localities in Juina, Brazil, and the diamonds were interpreted to be derived from the deep mantle [10,11]. Two different occurrences of titanomagnetites as the diamond inclusions have been reported: one was a titanomagnetite-bearing mineral composite, and the other was separate single-phase inclusions of titanomagnetite. As the former-type inclusion, Walter et al. [10] discovered a $\sim 30 \mu\text{m}$ -sized composite consisting mostly of orthopyroxene together with olivine and titanomagnetite (called “ulvöspinel” in their study) in a diamond from the Juina-5 kimberlite, Brazil. The analyzed composition of the titanomagnetite was approximately 36 mol % Fe_2TiO_4 ·36 mol % Fe_3O_4 ·28 mol % Mg_2TiO_4 . Walter et al. [10] interpreted that the three-phase composite was originally a homogeneous Mg-rich bridgmanite in the lower mantle, and that the diamond was transported to the upper mantle at a depth range of ~ 150 – 200 km where immiscibility into the three phases occurred before eruption of the kimberlite. Based on the experimental data on $\text{NaAlSi}_3\text{O}_8$ – MgAl_2O_4 [42,43], Walter et al. [10] estimated the depth range of ~ 150 – 200 km using nepheline–spinel composite inclusions which were interpreted to be originally calcium ferrite (CF)-type phase and hexagonal aluminous (NAL) phase in the lower mantle and the unmixing occurred at the depth range. Figures 1 and 3 and the results of Woodland et al. [44] indicate that the upper bound of stability field of Sp-type Mg_2TiO_4 , Fe_2TiO_4 and Fe_3O_4 increases in the order of ~ 1 , ~ 4 and $\sim 10 \text{ GPa}$, respectively. Using the pressures, we roughly estimate the upper limit of stability field of the titanomagnetite inclusion of the above composition to be ~ 5 – 6 GPa . The pressure is compatible with the estimated depth range of ~ 150 – 200 km from the CF and NAL inclusions.

The other kind of titanomagnetites was separate single-phase inclusions in superdeep diamonds. By a new combined method of synchrotron microtomography and single-crystal X-ray diffraction with fast, non-destructive methodology, Wenz et al. [11] discovered ~ 10 – $20 \mu\text{m}$ -sized inclusions of separate titanomagnetite crystals and powders in diamonds from São Luiz, Juina, Brazil. They observed that titanomagnetite inclusions were relatively abundant next to (Mg,Fe)O magnesio-wüstite and $\text{Fe}_{2-x}\text{Ti}_x\text{O}_3$ titanohematite, and determined lattice parameters of the titanomagnetites embedded in the diamonds to be 8.511 – 8.405 \AA by in situ X-ray diffraction method. Wenz et al. [11] assumed that compositions of the titanomagnetites were on the join Fe_2TiO_4 – Fe_3O_4 , because chemical analysis of the titanomagnetites was not made in the study. However, it is likely that the titanomagnetites contained minor amounts of Mg_2TiO_4 and MgFe_2O_4 components, as that found by Walter et al. [10]. At ambient conditions, cell parameters of Fe_2TiO_4 Sp and Fe_3O_4 Sp are $8.5375(3) \text{ \AA}$ (this study) and $8.3984(8) \text{ \AA}$ [4], respectively, while Mg_2TiO_4 Sp and MgFe_2O_4 Sp are $8.4398(1) \text{ \AA}$ (this study) and 8.391 \AA [45], respectively. Therefore, there is large uncertainty in estimating compositions of the titanomagnetites in the diamonds only from the lattice parameters determined by the in situ measurements. It should

also be considered that remnant pressure probably remained in the titanomagnetites embedded in the diamonds. When we use measured bulk modulus of Fe_2TiO_4 Sp of 121 GPa [8,46] or 147 GPa [47], the pressure dependence of cell parameter is calculated to be -0.023 or -0.019 Å/GPa, respectively.

We suggest, however, that the remnant pressure and possible presence of Mg_2TiO_4 and MgFe_2O_4 components, if any, decrease the lattice parameter of titanomagnetite from that in the Fe_2TiO_4 – Fe_3O_4 system at 1 atm. When we assume that the titanomagnetites in the diamonds are Mg-free solid solutions in the system Fe_2TiO_4 – Fe_3O_4 and the remnant pressure is negligibly small, we can estimate 81 mol % of Fe_2TiO_4 component for the titanomagnetite with the largest cell parameter ($a = 8.511$ Å). Because this is the lower bound for the Fe_2TiO_4 component, as discussed above, it is probable that the titanomagnetite composition was more Fe_2TiO_4 -rich, possibly almost pure Fe_2TiO_4 . Such titanomagnetites of very high Fe_2TiO_4 content probably could not be directly incorporated at a depth where the diamonds were formed, because the graphite–diamond transition boundary [36] is placed by ~ 1 GPa at higher pressure than the upper bound of the stability field of Fe_2TiO_4 Sp (Figure 4). Therefore, the above estimate would suggest that the Fe_2TiO_4 -rich titanomagnetites were originally CT-type phases which are stable above ~ 15 GPa in the transition zone and the lower mantle conditions, and that they back-transformed to the Fe_2TiO_4 -rich titanomagnetites in the diamonds after being transported to the upper mantle. The decomposition into FeTiO_3 Ilm (or Pv) + FeO Wu might have been kinetically hindered. Further experimental studies, particularly compositional analysis of the titanomagnetites, would be required to better clarify the origin of the titanomagnetites in the superdeep diamonds.

Author Contributions: T.T., M.O. and M.A. conducted the experiments; T.T., M.O., H.K. and M.A. analyzed the obtained data; M.A. and H.K. wrote the manuscript.

Funding: This work was supported in part by JSPS KAKENHI (grant nos. 25287145 and 17H02986 to M.A.) and by the MEXT-supported program of Gakushuin University for the Strategic Research Foundation at Private Universities.

Acknowledgments: I (M.A.) thank Robert C. Liebermann (Bob-san) for his suggestion to submit the paper to the Special Issue, Mineral Physics–In Memory of Orson Anderson, and for his encouragements on various occasions to me. We are grateful to T. Ishii, H. Yusa, D. Mori and Y. Inaguma for useful suggestions and discussion.

Conflicts of Interest: The authors declare no conflict of interest.

References

1. Wechsler, B.A.; Lindsley, D.H.; Prewitt, C.T. Crystal structure and cation distribution in titanomagnetites ($\text{Fe}_{3-x}\text{Ti}_x\text{O}_4$). *Am. Mineral.* **1984**, *69*, 754–770.
2. Yamanaka, T.; Mine, T.; Asogawa, S.; Nakamoto, Y. Jahn-Teller transition of Fe_2TiO_4 observed by maximum entropy method at high pressure and low temperature. *Phys. Rev.* **2009**, *B80*, 134120. [[CrossRef](#)]
3. Wechsler, B.A.; Von Dreele, R.B. Structure refinements of Mg_2TiO_4 , MgTiO_3 and MgTi_2O_5 by time-of-flight neutron powder diffraction. *Acta Cryst.* **1989**, *B45*, 542–549. [[CrossRef](#)]
4. Yamanaka, T.; Kyono, A.; Nakamoto, Y.; Meng, Y.; Kharlamova, S.; Struzhkin, V.V.; Mao, H.K. High-pressure phase transitions of $\text{Fe}_{3-x}\text{Ti}_x\text{O}_4$ solid solution up to 60 GPa correlated with electronic spin transition. *Am. Mineral.* **2013**, *98*, 736–744. [[CrossRef](#)]
5. Wu, Y.; Wu, X.; Qin, S. Pressure-induced phase transition of Fe_2TiO_4 : X-ray diffraction and Mössbauer spectroscopy. *J. Solid State Chem.* **2012**, *185*, 72–75. [[CrossRef](#)]
6. Xu, W.M.; Hearne, G.R.; Layek, S.; Levy, D.; Itie, J.-P.; Pasternak, M.P.; Rozenberg, G.K.; Greenberg, E. Site-specific spin crossover in Fe_2TiO_4 post-spinel under high pressure up to nearly a megabar. *Phys. Rev.* **2017**, *B96*, 045108. [[CrossRef](#)]
7. Akimoto, S.; Syono, Y. High-pressure decomposition of some titanate spinels. *J. Chem. Phys.* **1967**, *47*, 1813–1817. [[CrossRef](#)]
8. Liebermann, R.C.; Jackson, I.; Ringwood, A.E. Elasticity and phase equilibria of spinel disproportionation reactions. *Geophys. J. R. Astr. Soc.* **1977**, *50*, 553–586. [[CrossRef](#)]
9. Anderson, O.L. *Equations of State of Solids for Geophysics and Ceramic Science*; Oxford Univ. Press: New York, NY, USA, 1995; 405p.

10. Walter, M.J.; Kohn, S.C.; Araujo, D.; Bulanova, G.P.; Smith, C.B.; Gaillou, E.; Wang, J.; Steele, A.; Shirey, S.B. Deep mantle cycling of oceanic crust: Evidence from diamonds and their mineral inclusions. *Science* **2011**, *334*, 54–57. [[CrossRef](#)]
11. Wenz, M.D.; Jacobsen, S.D.; Zhang, D.; Regier, M.; Bausch, H.J.; Dera, P.K.; Rivers, M.; Eng, P.; Shirey, S.B.; Pearson, D.G. Fast identification of mineral inclusions in diamond at GSECARS using synchrotron X-ray microtomography, radiography and diffraction. *J. Synchrotron Rad.* **2019**, *26*, 1–6. [[CrossRef](#)]
12. Ito, E. Theory and Practice—Multianvil cells and high-pressure experimental methods. In *Mineral Physics*; Price, G.D., Ed.; Elsevier: Amsterdam, The Netherlands, 2007; Volume 2, pp. 197–230.
13. Dunn, K.J.; Bundy, F.P. Materials and techniques for pressure calibration by resistance-jump transitions up to 500 kilobars. *Rev. Sci. Instrum.* **1978**, *49*, 365–370. [[CrossRef](#)] [[PubMed](#)]
14. Morishima, H.; Kato, T.; Suto, M.; Ohtani, E.; Urakawa, S.; Utsumi, W.; Shimomura, O.; Kikegawa, T. The phase boundary between α - and β -Mg₂SiO₄ determined by in situ X-ray observation. *Science* **1994**, *265*, 1202–1203. [[CrossRef](#)] [[PubMed](#)]
15. Suzuki, A.; Ohtani, E.; Morishima, H.; Kubo, T.; Kanbe, Y.; Kondo, T. In situ determination of the phase boundary between wadsleyite and ringwoodite in Mg₂SiO₄. *Geophys. Res. Lett.* **2000**, *27*, 803–806. [[CrossRef](#)]
16. Fei, Y.; Van Orman, J.; Li, J.; Van Westrenen, W.; Sanloup, C.; Minarik, W.; Hirose, K.; Komabayashi, T. Experimentally determined post-spinel transformation boundary in Mg₂SiO₄ using MgO as an internal pressure standard and its geophysical implications. *J. Geophys. Res.* **2004**, *109*. [[CrossRef](#)]
17. Linton, J.A.; Fei, Y.; Navrotsky, A. The MgTiO₃-FeTiO₃ join at high pressure and temperature. *Am. Mineral.* **1999**, *84*, 1595–1603. [[CrossRef](#)]
18. El Goresy, A.; Chen, M.; Dubrovinsky, L.; Gillet, P.; Graup, G. An ultradense polymorph of rutile with seven-coordinated titanium from the Ries Crater. *Science* **2001**, *293*, 1467–1470. [[CrossRef](#)] [[PubMed](#)]
19. El Goresy, A.; Dubrovinsky, L.; Gillet, P.; Graup, G.; Chen, M. Akaogiite: An ultra-dense polymorph of TiO₂ with the baddeleyite-type structure, in shocked garnet gneiss from the Ries Crater, Germany. *Am. Mineral.* **2010**, *95*, 892–895. [[CrossRef](#)]
20. Akaogi, M.; Kusaba, K.; Susaki, J.; Yagi, T.; Matsui, M.; Kikegawa, T.; Yusa, H.; Ito, E. High-pressure high-temperature stability of α PbO₂-type TiO₂ and MgSiO₃ majorite: Calorimetric and in situ x-ray diffraction studies. In *High-Pressure Research: Application to Earth and Planetary Sciences*; Syono, Y., Manghnani, M.H., Eds.; Am. Geophys. Union: Washington, DC, USA, 1992; pp. 447–455.
21. Tang, J.; Endo, S. P-T boundary of α -PbO₂ type and baddeleyite type high-pressure phases of titanium dioxide. *J. Am. Ceram. Soc.* **1993**, *76*, 796–798. [[CrossRef](#)]
22. Kojitani, H.; Yamazaki, M.; Kojima, M.; Inaguma, Y.; Mori, D.; Akaogi, M. Thermodynamic investigation of the phase equilibrium boundary between TiO₂ rutile and its α -PbO₂-type high-pressure polymorph. *Phys. Chem. Min.* **2018**, *45*, 963–980. [[CrossRef](#)]
23. Dubrovinskaia, N.A.; Dubrovinsky, L.S.; Ahuja, R.; Prakapenka, V.B.; Dmitriev, V.; Weber, H.P.; Osorio-Guillen, J.M.; Johansson, B. Experimental and theoretical identification of a new high-pressure TiO₂ polymorph. *Phys. Rev. Lett.* **2001**, *87*, 275501. [[CrossRef](#)]
24. Al-Khatatbeh, Y.; Lee, K.K.M.; Kiefer, B. High-pressure behavior of TiO₂ as determined by experiment and theory. *Phys. Rev.* **2009**, *B79*, 134114. [[CrossRef](#)]
25. Akaogi, M.; Arai, S.; Abe, K.; Kojitani, H. Unpublished work. 2018.
26. Akaogi, M.; Abe, K.; Yusa, H.; Ishii, T.; Tajima, T.; Kojitani, H.; Mori, D.; Inaguma, Y. High-pressure high-temperature phase relations in FeTiO₃ up to 35 GPa and 1600 °C. *Phys. Chem. Min.* **2017**, *44*, 63–73. [[CrossRef](#)]
27. Leinenweber, K.; Utsumi, W.; Tsuchida, Y.; Yagi, T.; Kurita, K. Unquenchable high-pressure perovskite polymorphs of MnSnO₃ and FeTiO₃. *Phys. Chem. Min.* **1991**, *18*, 244–250. [[CrossRef](#)]
28. Dubrovinsky, L.; El Goresy, A.; Gillet, P.; Wu, X.; Simionivici, A. A novel natural shock-induced high-pressure polymorph of FeTiO₃ ilmenite with the Li-niobate structure from the Ries crater, Germany. *Meteorit. Planet. Sci.* **2009**, *44*, A64.
29. Xie, X.; Gu, X.; Yang, H.; Chen, M.; Li, K. Wangdaodeite. IMA 2016-007. CNMNC Newsletter, No. 31. *Mineral. Mag.* **2016**, *80*, 691–697.
30. Nishio-Hamane, D.; Zhang, M.; Yagi, T.; Ma, Y. High-pressure and high-temperature phase transitions in FeTiO₃ and a new dense FeTi₃O₇ structure. *Am. Mineral.* **2012**, *97*, 568–572. [[CrossRef](#)]

31. Hazen, R.M. Effects of temperature and pressure on the cell dimension and X-ray temperature factors of periclase. *Am Mineral.* **1976**, *66*, 266–271.
32. Linton, J.A.; Fei, Y.; Navrotsky, A. Complete Fe-Mg solid solution in lithium niobate and perovskite structures in titanates at high pressures and temperatures. *Am. Mineral.* **1997**, *82*, 639–642. [[CrossRef](#)]
33. Nishio-Hamane, D.; Shimizu, A.; Nakahira, R.; Niwa, K.; Sano-Furukawa, A.; Okada, T.; Yagi, T.; Kikegawa, T. The stability and equation of state for the cotunnite phase of TiO₂ up to 70 GPa. *Phys. Chem. Min.* **2010**, *37*, 129–136. [[CrossRef](#)]
34. McCammon, C.A. Effect of pressure on the composition of the lower mantle end member Fe_xO. *Science* **1993**, *259*, 66–68. [[CrossRef](#)]
35. Ming, L.C.; Kim, Y.H.; Uchida, T.; Wang, Y.; Rivers, M. In situ X-ray diffraction study of phase transitions of FeTiO₃ at high pressures and temperatures using a large-volume press and synchrotron radiation. *Am. Mineral.* **2006**, *91*, 120–126. [[CrossRef](#)]
36. Kennedy, C.S.; Kennedy, G.C. The equilibrium boundary between graphite and diamond. *J. Geophys. Res.* **1976**, *81*, 2467–2470. [[CrossRef](#)]
37. Yamanaka, T.; Uchida, A.; Nakamoto, Y. Structural transition of post-spinel phases CaMn₂O₄, CaFe₂O₄, and CaTi₂O₄ under high pressure up to 80 GPa. *Am. Mineral.* **2008**, *93*, 1874–1881. [[CrossRef](#)]
38. Ishii, T.; Kojitani, H.; Tsukamoto, S.; Fujino, K.; Mori, D.; Inaguma, Y.; Tsujino, N.; Yoshino, T.; Yamazaki, D.; Higo, Y. High-pressure phase transitions in FeCr₂O₄ and structure analysis of new post-spinel FeCr₂O₄ and Fe₂Cr₂O₅ phases with meteoritical and petrological implications. *Am. Mineral.* **2014**, *99*, 1788–1797. [[CrossRef](#)]
39. Shannon, R.D. Revised effective ionic radii and systematic studies of interatomic distances in halides and chalcogenides. *Acta Cryst.* **1976**, *A32*, 751–767. [[CrossRef](#)]
40. Oganov, A.R. Thermodynamics, phase transitions, equations of state, and elasticity of minerals at high pressures and temperatures. In *Mineral Physics*, 2nd ed.; Price, G.D., Ed.; Elsevier: Amsterdam, The Netherlands, 2015; Volume 2, pp. 179–201.
41. Momma, K.; Izumi, F. VESTA 3 for three-dimensional visualization of crystal, volumetric and morphology data. *J. Appl. Crystallogr.* **2011**, *44*, 1272–1276. [[CrossRef](#)]
42. Akaogi, M.; Tanaka, A.; Kobayashi, M.; Fukushima, N.; Suzuki, T. High-pressure transformations in NaAlSiO₄ and thermodynamic properties of jadeite, nepheline, and calcium ferrite-type phase. *Phys. Earth Planet. Inter.* **2002**, *130*, 49–58. [[CrossRef](#)]
43. Ono, A.; Akaogi, M.; Kojitani, H.; Yamashita, K.; Kobayashi, M. High-pressure phase relations and thermodynamic properties of hexagonal aluminous phase and calcium-ferrite phase in the systems NaAlSiO₄-MgAl₂O₄ and CaAl₂O₄-MgAl₂O₄. *Phys. Earth Planet. Inter.* **2009**, *174*, 39–49. [[CrossRef](#)]
44. Woodland, A.B.; Frost, D.J.; Trots, D.M.; Klimm, K.; Mezouar, M. In situ observation of the breakdown of magnetite (Fe₃O₄) to Fe₄O₅ and hematite at high pressures and temperatures. *Am. Mineral.* **2012**, *97*, 1808–1811. [[CrossRef](#)]
45. O'Neill, H.S.C.; Annersten, H.; Virgo, D. The temperature dependence of the cation distribution in magnesioferrite (MgFe₂O₄) from powder XRD structural refinements and Mössbauer spectroscopy. *Am. Mineral.* **1992**, *77*, 725–740.
46. Syono, Y.; Fukai, Y.; Ishikawa, Y. Anomalous elastic properties of Fe₂TiO₄. *J. Phys. Soc. Jpn.* **1971**, *31*, 471–476. [[CrossRef](#)]
47. Xiong, Z.; Liu, X.; Shieh, S.R.; Wang, F.; Wu, X.; Hong, X.; Shi, Y. Equation of state of a synthetic ulvöspinel, (Fe_{1.94}Ti_{0.03})Ti_{1.00}O_{4.00}, at ambient temperature. *Phys. Chem. Miner.* **2015**, *42*, 171–177. [[CrossRef](#)]

